

Multipolar Force Fields for Amide-I Spectroscopy from Conformational Dynamics of the Alanine-Trimer

Padmabati Mondal,^{*,†,¶} Pierre-André Cazade,^{†,§} Akshaya K. Das,^{†,||} Tristan
Bereau,^{†,⊥} and Markus Meuwly^{*,†,‡}

[†]*Department of Chemistry, University of Basel, Klingelbergstrasse 80, 4056 Basel,
Switzerland*

[‡]*Department of Chemistry, Brown University, Providence/RI, USA*

[¶]*Current address: Department of Chemistry and Center for Atomic, Molecular and Optical
Sciences and Technologies, Indian Institute of Science Education and Research (IISER)
Tirupati, Karakambadi Road, Mangalam, Tirupati-517507, Andhra Pradesh, India.*

[§]*Current address: Bernal Institute, University of Limerick, Plassey Park Road, co.
Limerick, Castletroy, Ireland*

E-mail: padmabati.mondal@iisertirupati.ac.in; m.meuwly@unibas.ch

June 21, 2021

Abstract

The dynamics and spectroscopy of N-methyl-acetamide (NMA) and trialanine in solution is characterized from molecular dynamics (MD) simulations using different energy functions, including a conventional point charge (PC)-based force field, one based on a multipolar (MTP) representation of the electrostatics, and a semiempirical DFT method. For the 1-d infrared spectra, the frequency splitting between the two amide-I groups is 10 cm^{-1} from the PC, 13 cm^{-1} from the MTP, and 47 cm^{-1} from SCC-DFTB simulations, compared with 25 cm^{-1} from experiment. The frequency trajectory required for determining the frequency fluctuation correlation function (FFCF) is determined from individual (INM) and full normal mode (FNM) analyses of the amide-I vibrations. The spectroscopy, time-zero magnitude of the FFCF $C(t=0)$, and the static component Δ_0^2 from simulations using MTP and analysis based on FNM are all consistent with experiments for (Ala)₃. Contrary to that, for the analysis excluding mode-mode coupling (INM) the FFCF decays to zero too rapidly and for simulations with a PC-based force field the Δ_0^2 is too small by a factor of two compared with experiments. Simulations with SCC-DFTB agree better with experiment for these observables than those from PC-based simulations. The conformational ensemble sampled from simulations using PCs is consistent with the literature (including P_{II} , β , α_R , and α_L), whereas that covered by the MTP-based simulations is dominated by P_{II} with some contributions from β , α_R . This agrees with and confirms recently reported, Bayesian-refined populations based on 1-dimensional infrared experiments. Full normal mode analysis together with a MTP representation provides a meaningful model to correctly describe the dynamics of hydrated trialanine.

Introduction

Ultrafast Infrared (IR) spectroscopy is a powerful tool to characterize the solvent dynamics around chromophores on the pico- and sub-picosecond time scale. It has also been

proven to be a promising tool for studying the structure and dynamics of proteins, including protein-folding and protein-ligand binding.¹⁻⁷ The amide-I mode is suitable to probe the structural dynamics and the conformational ensemble of a solvated molecule, peptide, or protein.^{1,8} Other suitable vibrational labels^{9,10} that absorb in the spectroscopic window between ~ 1700 and $\sim 2800\text{ cm}^{-1}$ are cyanophenylalanine,¹¹ nitrile-derivatized amino acids,¹² the sulfhydryl band of cysteines,¹³ deuterated carbons,¹⁴ non-natural labels consisting of metal-tricarbonyl modified with a $-(\text{CH}_2)_n$ - linker,¹⁵ nitrile labels,¹⁶ cyano¹⁷ and SCN¹⁸ groups, or cyanamide.¹⁹ Contrary to these other probes the amide-I band characterizes the inherent dynamics of the system because it does not require mutation or chemical modification of the molecule considered.

N-methyl acetamide (NMA) is a typical model system for experimental,²⁰⁻²⁴ and computational²⁵⁻²⁸ studies because it is also the fundamental building block to study longer peptides and proteins. In going from a mono- to a poly-peptide one essentially moves from NMA to alanine dipeptide, to trialanine and to larger alanine chains. Therefore, to develop and validate force fields for the amide probe and to apply them to larger polypeptide chains, starting from NMA is a meaningful choice. This also allows one to assess the transferability of the force fields from NMA by using them for polypeptides and comparing the results with experimental data.

Two-dimensional infrared (2D-IR) spectroscopy provides quantitative information about the solvent structure and dynamics surrounding a solute.²⁹ Such techniques are particularly useful to measure the fast (picosecond) dynamics in condensed-phase systems. The coupling between inter- and intramolecular degrees of freedom - such as the hydrogen bonding network in solution, or the conformational dynamics of biological macromolecules - can be investigated by monitoring the fluctuation of a fundamental vibrational frequency, which is the amide-I mode in the present work. Computationally, this information is accessible

from either instantaneous normal modes (NM),^{5,25,30} the solution of a reduced-dimensional nuclear Schrödinger equation,^{31,32} or from spectroscopic maps.³³ This frequency trajectory ($\omega(t)$ or $\nu(t)$ for harmonic or anharmonic vibrations, respectively) is then used to determine the frequency fluctuation correlation function which can be directly compared with experimental measurements.

The linear and non-linear vibrational spectroscopy and conformational dynamics of trialanine in solution has been investigated from both, experiments and computations.³⁴⁻⁴⁴ Computationally, a quantum-classical description of the amide-I vibrational spectrum of trialanine in D₂O probed different approximations typically made in determining the vibrational line-shapes.⁴¹ A combined experimental and molecular dynamical study using non-linear time-resolved spectroscopy on trialanine found conformational heterogeneity of the peptide.³⁵ Peptide conformational ensembles were also studied for trialanine using two-dimensional IR and NMR spectroscopies.⁴²⁻⁴⁴ Two-dimensional IR studies probed the subpicosecond dynamics³⁶ and with isotopically labelled (Ala)₃ the dipole-dipole coupling strength was determined.³⁸ Including such couplings is often done in models based on spectroscopic maps. In the present work, NMs are determined from “independent normal modes” (INM) and from a “full normal mode” (FNM) analysis which allows coupling of two or several amide-I modes.

The present work is structured as follows. First, the methods used are introduced. This is followed by an analysis the spectroscopy and dynamics of solvated, deuterated N-methylacetamide with a flexible solute. Next, the spectroscopy and structural dynamics of trialanine are discussed. Finally, conclusions are drawn.

Computational methods

Molecular Dynamics Simulations

Molecular Dynamics (MD) simulations were carried out for N-deuterated N-methylacetamide (NMAD, see Figure 1) and trialanine (Ala)₃ in a periodic cubic box of deuterated TIP3P⁴⁵ water molecules. The box size was 30³ Å³ and the system consisted of one solute molecule surrounded by 882 water molecules (for NMAD) and 795 water molecules (for (Ala)₃), respectively. (Ala)₃ was fully deuterated and the positively charged species (i.e. “cationic” with ND₃⁺ and COOD termini) was investigated.^{34,44} To neutralize the simulation system, one chloride ion was added and constrained in one corner of the simulation system during MD simulations.

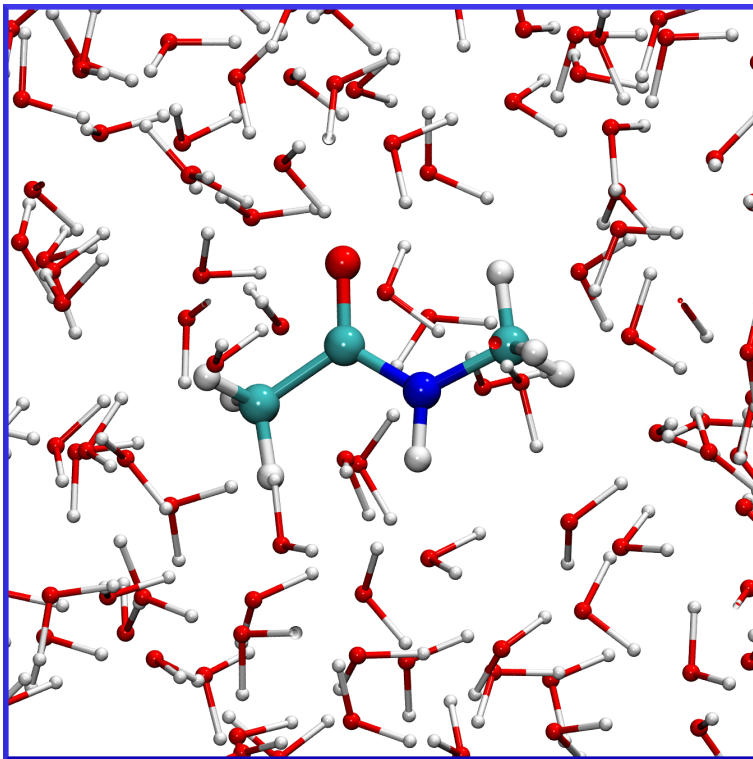


Figure 1: N-methylacetamide (NMAD) solvated in a periodic cubic box of D₂O of size 30³ Å³. Atom color code: Carbon (cyan), Oxygen (red), Nitrogen (blue) and Hydrogen (white).

All MD simulations were performed with the CHARMM program⁴⁶ with provision for mul-

tipolar interactions.^{47,48} Parameters for NMA are based on CGenFF⁴⁹ unless stated otherwise and described in more detail in Ref.²⁵ Electrostatic interactions were treated using Particle-Mesh Ewald (PME)⁵⁰ with a grid-size spacing of 1 Å, characteristic reciprocal length $\kappa = 0.43 \text{ Å}^{-1}$, and interpolation order 4 for long-range electrostatics. For the Lennard-Jones (LJ) interactions a 12 Å cut-off and 10 Å switching were used. The simulations were performed at $T = 300 \text{ K}$ and all bonds involving hydrogen atoms were constrained via the SHAKE algorithm.⁵¹ The timestep was $\Delta t = 0.5 \text{ fs}$ and snapshots were recorded every 10 time steps.

Mixed QM/MM were carried out using Self-consistent charge density functional tight-binding (SCC-DFTB)⁵² as implemented in CHARMM.⁵³ In these simulations, the entire solute (NMAD or (Ala)₃) was treated with SCC-DFTB whereas all water molecules and the ion (for the solvated (Ala)₃ system) were treated by MM. First the system was minimized and heated to 300 K. A *NVT* simulation was carried out at 300 K using the velocity Verlet integrator with a (shorter) time step of $\Delta t = 0.25 \text{ fs}$ for 5 ns. Again, all bonds involving hydrogen atoms were constrained using SHAKE⁵¹ and the treatment of the nonbonded interactions was that same as that for the PC and MTP simulations described above.

Force fields for flexible NMA

Two different electrostatic models for NMA are used in this work. The first one uses point charges (PCs) based on the CGenFF force field. The second model is the multipolar MTPW representation including atomic multipoles up to quadrupoles on heavy atoms for the entire NMAD molecule.²⁵ The force field parameters for the CO bond are based on *ab initio* calculations at the MP2/6-31G** level and are readjusted to reproduce the gas phase amide-I frequency. The Morse parameters are $D_e = 141.67 \text{ kcal mol}^{-1}$, $\beta = 2.11 \text{ Å}^{-1}$ and $r_{\text{eq}} = 1.23 \text{ Å}$.

The parametrization for (Ala)₃ uses the CGenFF force field⁵⁴ except for the CO-stretch potential which is the same Morse function used for the -CO group of NMAD and the multipoles on the C-terminal CO atoms as well as outer and central [CONH] atoms which were also used for [CONH] group of NMAD.

The Frequency Fluctuation Correlation Function and 1D infrared spectrum

The FFCF, $C(t)$, is obtained from the frequency trajectory $\omega(t)$ according to:

$$\begin{aligned} C(t) &= \langle \delta\omega(t_0) \delta\omega(t_0 + t) \rangle_{t_0} \\ &= \langle (\omega(t_0) - \bar{\omega}) (\omega(t_0 + t) - \bar{\omega}) \rangle_{t_0} . \end{aligned} \tag{1}$$

Here, $\omega(t_0)$ is the instantaneous frequency at time t_0 and $\bar{\omega}$ is the average frequency and thereby $\delta\omega(t_0)$ refers to the frequency fluctuation at time t_0 . The instantaneous frequencies $\omega(t)$ are obtained from normal mode (NM) calculations. For each snapshot of the trajectory, the structure of the solute (here NMAD and (Ala)₃) is minimized while keeping the solvent frozen. Frequencies are calculated using two different approaches referred to as “full NM” (FNM) and “independent NM” (INM) analysis methods. For FNM the normal mode analysis is carried out for the entire solute. Such an approach includes both, the frequencies of the labels (“site energies”) and the couplings between them. On the other hand, INM refers to the normal mode analysis of the independent amide modes of trialanine while keeping everything except the [CONH] group fixed and therefore neglects the couplings between the spectroscopic labels. This approach is computationally more efficient than scanning along the normal mode and solving the 1- or even 3-dimensional nuclear Schrödinger equation.^{8,31,55}

The analysis adopted here is also reminiscent of instantaneous normal modes (NM) which have been shown to perform well for the short-time dynamics in condensed phase.⁵⁶⁻⁵⁹ Furthermore, a direct comparison between instantaneous normal modes, scanning (“scan”) along the local and normal mode and map-based frequency trajectories has been recently presented and found that “NM” and “scan” yield comparable FFCFs and 1d-lineshapes derived from them.⁸

The 1D and 2D response functions can be determined from the lineshape function $g(t)$,^{20,60} which is related to the FFCF through

$$g(t) = \int_0^t \int_0^{\tau'} d\tau' d\tau'' \langle \delta\omega(\tau'') \delta\omega(0) \rangle. \quad (2)$$

Depending on whether or not the FFCF is fit to a parametrized form, the double integration can be carried out in closed form or needs to be done numerically. In the present case, the functional form fitted to is

$$C(t) = \sum_{i=1}^n a_i \exp(-t/\tau_i) + \Delta_0^2 \quad (3)$$

with amplitudes a_i and decay times τ_i as fitting parameters and $n_{\max} = 2$ or 3 to make direct comparison with earlier work on (Ala)₃.⁶¹ The a_i and τ_i are amplitudes and relaxation times, respectively, and Δ_0^2 is the static component which can differ from 0 for situations in which processes occurring on longer time scales have not equilibrated on the time scales of the relaxation times τ_i .

Results

Spectroscopy of N-methylacetamide

To validate the energy functions and analysis techniques used subsequently for (Ala)₃ first the spectroscopy of NMAD in D₂O from MD simulations with PCs and MTPs for flexible solute were considered. In addition, QM(SCC-DFTB)/MM simulations were also carried out. For each of the three cases, 10⁶ snapshots from a 5 ns long trajectory were analyzed. For every snapshot the frequency, $\omega(t)$, was obtained from an instantaneous normal mode analysis. From this, the FFCFs were determined and fitted to multi-exponential decay functions along with a static component (Δ_0^2) according to Eq. 3 with $n_{\max} = 2$ or 3.

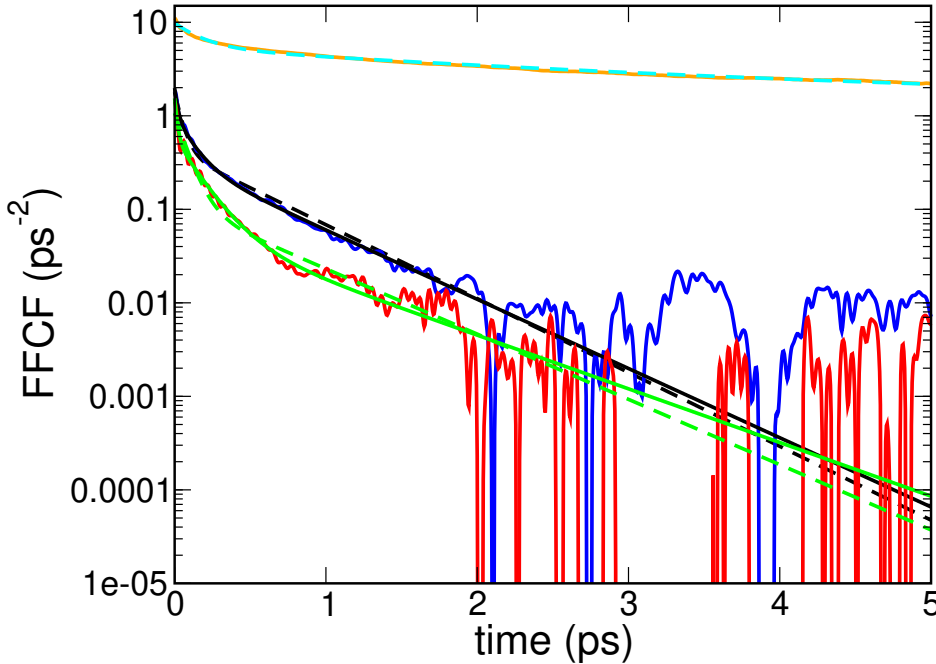


Figure 2: FFCFs for NMAD in D₂O (TIP3P) for simulations with PC (red), MTP (blue), and SCC-DFTB (orange) with flexible NMA. Green, black and cyan lines are fits to Eq. 3 for the FFCFs from simulations with PC, MTP, and SCC-DFTB, respectively. Dashed lines are for fits using $n_{\max} = 2$ and solid lines for fits with $n_{\max} = 3$ in Eq. 3.

Figure 2 shows the FFCF for NMAD in D₂O for the simulations with PC (red), MTP (blue), and SCC-DFTB (orange) models. The fits, using two or three time scales, respectively, are the dashed and solid green, black and cyan lines. The fitting parameters for the FFCFs are summarized in Table 1. Figure 2 shows that for the PC, MTP and SCC-DFTB, two time scales are sufficient to represent the FFCF. Also, for the two force field models the FFCFs decay to zero on the ~ 10 ps time scale whereas that from the SCC-DFTB simulations has a static component of $\Delta_0^2 = 1.3 \text{ ps}^{-2}$.

The short time decay τ_1 for the PC and MTP models range from 0.02 ps to 0.05 ps, consistent with experiments (between 0.01 and 0.1 ps).^{35,62} Contrary to that, simulations with SCC-DFTB yield $\tau_1 = 0.18$ ps which is at least a factor of two slower compared with what has been reported from experiments. The long time scale, τ_3 , ranges from 0.55 ps to 0.62 ps, compared with 1.0 ps and 1.6 ps from the experiments.^{35,62} Earlier MD simulations reported $\tau_3 = 0.66$ ps.⁶² The SCC-DFTB simulations find a long time scale $\tau_3 = 3.2$ ps which is longer than any of the experiments. It is also worthwhile to note that a two-time scale fit of the FFCF to the frequencies from the MTP simulation is sufficient and assuming three time scales does not provide additional information. This is also found from the experiments.⁶² The fits with only two time scales are preferred as with every additional time scale a new process is associated. For water the sub-picosecond time scale has been associated with partial water reorientation whereas the process on the ps time scale is considered to involve full water reorientation.⁶³

Table 1: Parameters of tri/bi-exponential fit (Eqn. 3) for MTP and PC models and bi-exponential plus static component fit (Eqn. 3) for SCC-DFTB calculations for the FFCFs of the carbonyl group of NMAD in D₂O for different models.

Model	a_1 [ps ⁻²]	τ_1 [ps]	a_2 [ps ⁻²]	τ_2 [ps]	a_3 [ps ⁻²]	τ_3 [ps]	Δ_0^2 [ps ⁻²]
PC	0.470	0.019	0.597	0.075	0.085	0.588	–
PC (bi-exp)	0.951	0.080	–	–	0.115	0.622	–
MTP	0.942	0.019	0.707	0.110	0.330	0.587	–
MTP (bi-exp)	1.361	0.049	–	–	0.418	0.550	–
SCC-DFTB	4.488	0.183	–	–	3.982	3.202	1.344
sim. ⁶²		0.06				0.66	
exp. ³⁵		(0.05-0.1)				1.6	
exp. ⁶²		0.01				1.0	

The 1D absorption spectra are calculated from the analytical integration^{5,64} of the lineshape function (see Eq. 2) with the FFCF ($C(t)$) fit to Eq. 3. A phenomenological broadening for the amide-I vibration consistent with a lifetime of 0.45 ps was used.²² The maxima of the 1D lineshape for NMAD in D₂O for PC, MTP and SCC-DFTB models are 1705 cm⁻¹, 1695 cm⁻¹ and 1695 cm⁻¹, respectively, see Figure 3. The gas phase frequency for amide mode of NMAD is 1717 cm⁻¹ and solvent induced red-shift for PC, MTP and SCC-DFTB models are 12 cm⁻¹, 22 cm⁻¹ and 22 cm⁻¹, respectively. This compares with an experimental solvent induced red-shift of 85 cm⁻¹.⁶⁵ The full width at half maximum (FWHM) of the calculated 1D absorption spectra (Figure 3) for NMAD in D₂O using the PC, MTP, and SCC-DFTB models are 12.5 cm⁻¹, 14 cm⁻¹, and 35 cm⁻¹, compared with ~ 20 cm⁻¹ from experiments.⁶¹

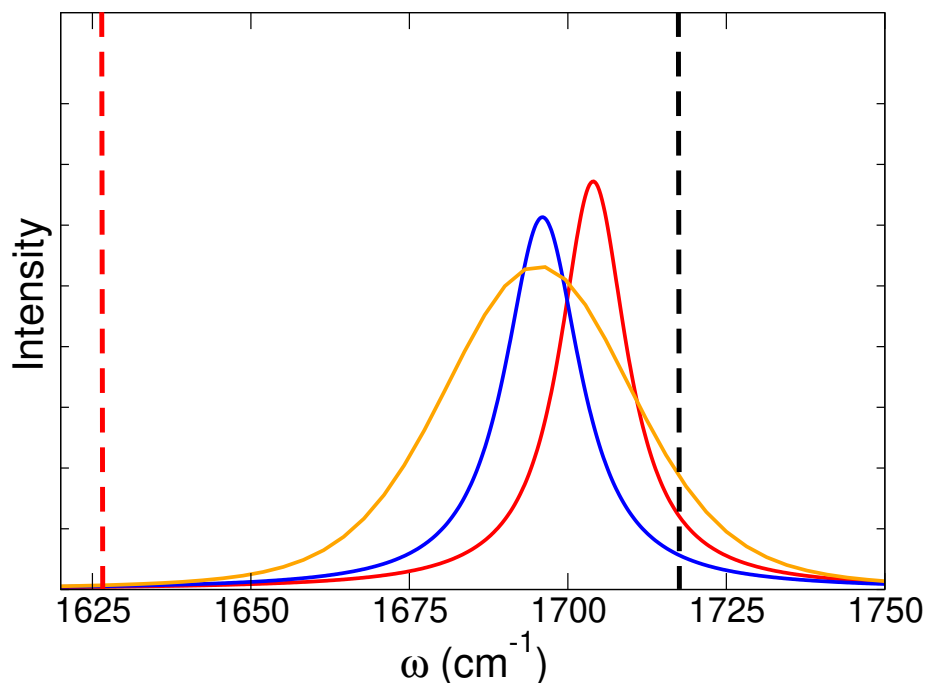


Figure 3: 1D absorption spectra of NMAD in D_2O in the region of the amide-I mode from simulations with the PC (red), MTP (blue), and the SCC-DFTB (orange) models. Experimental peaks for amide I mode of NMAD in D_2O and in the gas phase are shown as red and black dashed vertical line, respectively. The experimental solvent-induced red shift is 85 cm^{-1} .^{65,66}

In summary, the PC and MTP models correctly capture the short and long time scales compared with experiment with the MTP model performing somewhat better. Simulations with both force fields correctly find that the FFCFs decay to zero on the few-picosecond time scale whereas SCC-DFTB leads to a static component which was not found in the experiments. For the 1d-infrared spectroscopy, all models find a solvent-induced red shift which, however, underestimates the experimentally reported magnitude and the FWHM from MTP is closest to that observed experimentally.⁶¹

Spectroscopy and Dynamics of Trialanine

Next, the spectroscopy and dynamics of (Ala)₃ (see Figure 4) are considered. Trialanine involves two amide-I groups (central and outer -CO) and one terminal carboxylic (COOH) group. For each interaction model, 10 ns MD simulations were performed for deuterated trialanine in deuterated water using PC, MTP, and SCC-DFTB (validated for NMAD in D₂O). This was preceded by 1 ns of *NPT* equilibration and further 100 ps *NVT* equilibration. The -CO(OH) group of trialanine is characteristically different from the amide -CO group. To account for this a slightly modified Morse (β) parameter (than what has been used for C=O of NMAD in D₂O) is used for the C-terminal -CO group in the simulations and NM calculations.

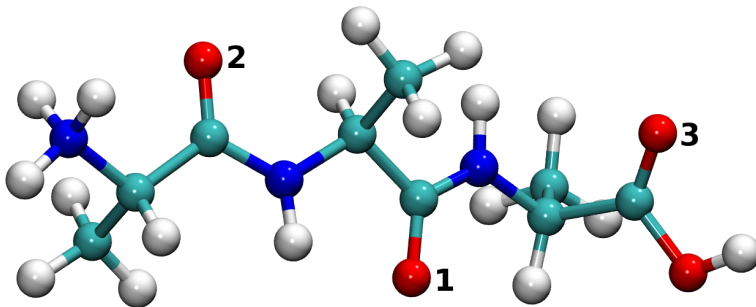


Figure 4: The structure of protonated (cationic) (Ala)₃.³⁴ The central (1), outer (2) and carboxylic (3) -CO groups are specifically labelled. Hydrogen (white), oxygen (red), nitrogen (blue), and carbon (cyan) are shown as spheres.

Frequency Distributions: Frequencies for the central and outer amide as well as terminal CO(OH) are calculated using both, FNM and INM analyses. The experimentally determined peak positions are at 1650 cm⁻¹, 1675 cm⁻¹ and 1725 cm⁻¹ for the central, outer and carboxylic -CO, respectively.³⁴ In the following, results from the FNM analysis are discussed first and then compared with those obtained from INMs, see Figure 8 and Table 2.

Figures 5A and B show the frequency distribution for the central (black), outer (red) and terminal (green) carbonyl group from simulations with the MTP and SCC-DFTB models, respectively. The down-headed arrows of corresponding color indicate the experimental³⁴

peak positions of each -CO group and the vertical dashed lines refer to the shifted experimental peak position to best overlap with the simulated data for the central -CO. This is meaningful because for the present work primarily *relative positions* of the absorption bands are of interest. Fine-tuning of the Morse parameters to match experimental line positions would still be possible for the PC and MTP models as an additional refinement but is not deemed necessary here.

For MTP a constant shift of 22 cm^{-1} to the blue from the experimental spectra yielded the best overlap for the central -CO peak. The computations find a frequency of 1673 cm^{-1} for the central -CO (black), followed by the outer -CO at 1686 cm^{-1} (red), and finally the -CO(OH) group at 1739 cm^{-1} (green). Although the same force field (MTP and Morse) was used for the central and outer amide, the different environments experienced by them leads to a splitting of 13 cm^{-1} . This sensitivity to the environmental structure and dynamics is consistent with recent findings for insulin monomer and dimer.⁸ Nevertheless, the experimentally observed splitting of 25 cm^{-1} is still underestimated.³⁴ The simulations with the PC model also yield the correct ordering for the frequencies of the central and outer -CO (at 1677 cm^{-1} , 1687 cm^{-1}) but the splitting is somewhat smaller (10 cm^{-1}) than that from the simulations using MTP.

It is conceivable that further improvements of the electrostatics^{67,68} leads to yet closer agreement between simulations and experiments. For one, conformationally dependent multipoles provide an even better description of the electrostatics as has been found for isolated CO in Mb.⁶⁹⁻⁷² Furthermore, including polarizability may lead to additional improvements.

With SCC-DFTB the central, outer and terminal carbonyl peaks are at 1648 cm^{-1} , 1695 cm^{-1} and 1598 cm^{-1} (Figure 5B, D). A constant shift of 5 cm^{-1} (red) from the experimental spectra was considered to best overlap the central -CO peak for the simulations with the

SCC-DFTB results. Consistent with experiment, the frequency of the outer -CO is shifted to the blue (+47 cm^{-1}) from the central -CO by close to twice the value reported from experiment (+25 cm^{-1}).³⁴ For the carbonyl (COOH) -CO, SCC-DFTB underestimates the frequency by 125 cm^{-1} compared with experiment. This finding was reproduced from two independent simulations. Upon visual inspection of the trajectories it was observed that the COOH unit is typically in an anti conformation whereas the minimum energy structure is the syn conformer. To further validate the performance of SCC-DFTB, simulations for (Ala)₃ in the gas phase using the mio^{52,73} and 3ob-freq⁷⁴ parameter sets were carried out. With the mio parameters, used for this study, the frequency distributions of the central and outer -CO label are split by $\sim 25 \text{ cm}^{-1}$ - to be compared with a splitting of 25 cm^{-1} from experiment in solution - whereas with the 3ob-freq parametrization - which was refined for thermochemistry, geometries, and vibrational frequencies in the gas phase - the splitting is 110 cm^{-1} . Hence, it is not expected that a different parametrization will appreciably improve the findings for simulations in solution.

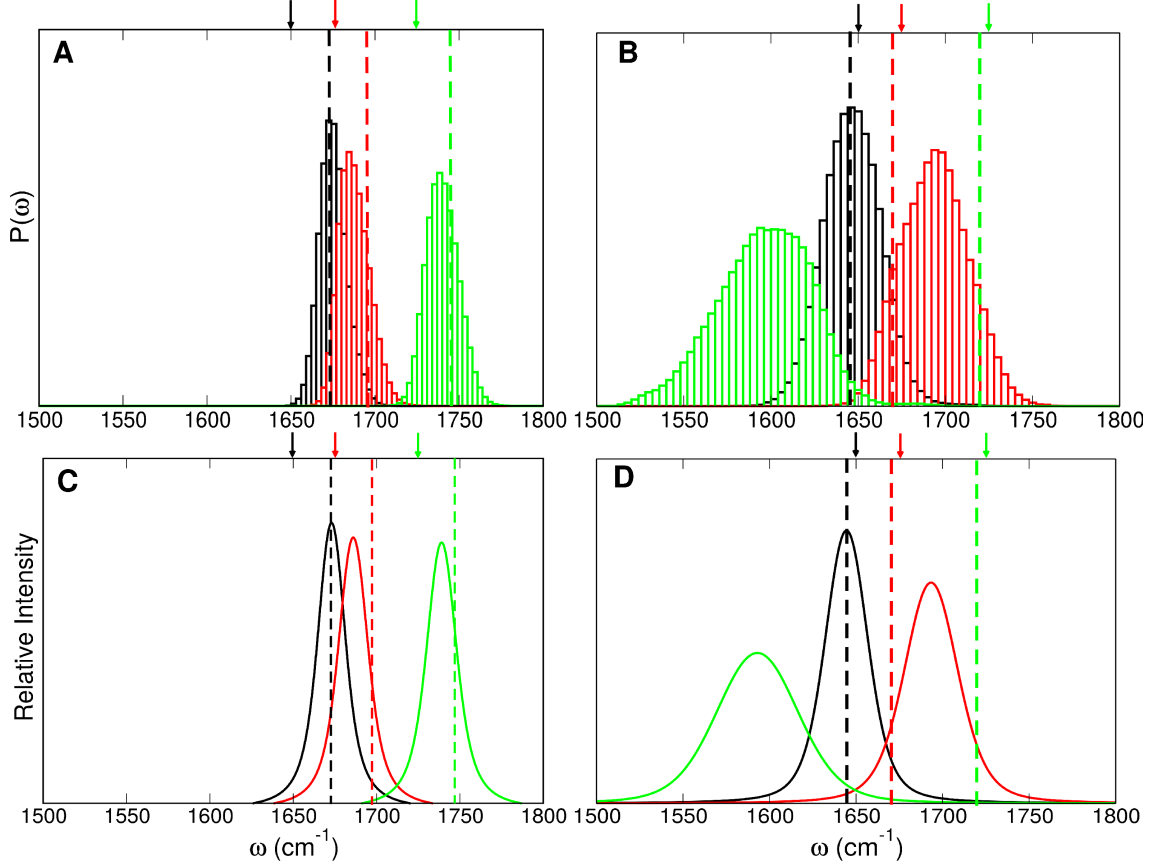


Figure 5: Frequency distributions (panels A and B) and 1D absorption spectra (panels C and D) of each -CO moiety of trialanine for the central (black), outer (red), and terminal (green) -CO. Panels A and C correspond to results using MTP and panels B and D to those from SCC-DFTB simulations. The down-headed arrows indicate the experimental³⁴ peak position of each -CO group whereas the vertical dashed lines with corresponding color show the shifted experimental peak position to best overlap with the simulated data of central -CO. A constant shift of 22 cm⁻¹ (blue) and 5 cm⁻¹ (red) from the experimental spectra was considered to best overlap the central -CO peak for the simulations with MTPs and SCC-DFTB, respectively.

Frequency Fluctuation Correlation Function: The frequency fluctuation correlation function provides information about the environmental dynamics surrounding a local spectroscopic probe and the coupling to it. The FFCFs were fitted to a bi-exponential decay with static component (equation 3) as has also been done for NMAD.⁶¹ The raw data with the corresponding fits are shown in Figure 6 and the parameters are summarized in Table 2. FFCFs for each -CO probe of trialanine using the MTP model (Figure 6A) and from SCC-DFTB simulations (Figure 6B) for central (black), outer (red), and terminal (green) -CO are re-

ported.

Table 2: Parameters for fitting the FFCFs to a bi-exponential decay with static component fit (Eqn. 3) for trialanine from simulations using the PC, MTP, and SCC-DFTB models.

Model	Mode	a_1 [ps^{-2}]	τ_1 [ps]	a_2 [ps^{-2}]	τ_2 [ps]	Δ_0^2 [ps^{-2}]
MTP (FNM)	-CO(central)	1.348	0.038	0.274	1.337	0.723
	-CO (outer)	1.709	0.044	0.373	3.066	0.797
	-CO(OH)	1.804	0.067	0.568	3.184	0.620
MTP (INM)	-CO (central)	2.250	0.057	0.662	1.043	0.087
	-CO(outer)	2.360	0.076	0.419	1.543	0.023
PC (FNM)	-CO (central)	1.391	0.039	0.204	2.306	0.200
	-CO (outer)	1.942	0.037	0.422	4.697	0.419
	-CO(OH)	1.465	0.098	1.350	6.028	0.099
SCC-DFTB (FNM)	-CO(central)	4.872	0.076	3.052	1.845	0.908
	-CO (outer)	4.981	0.124	6.299	1.350	0.468
	-CO(OH)	9.780	0.311	9.198	3.508	2.877

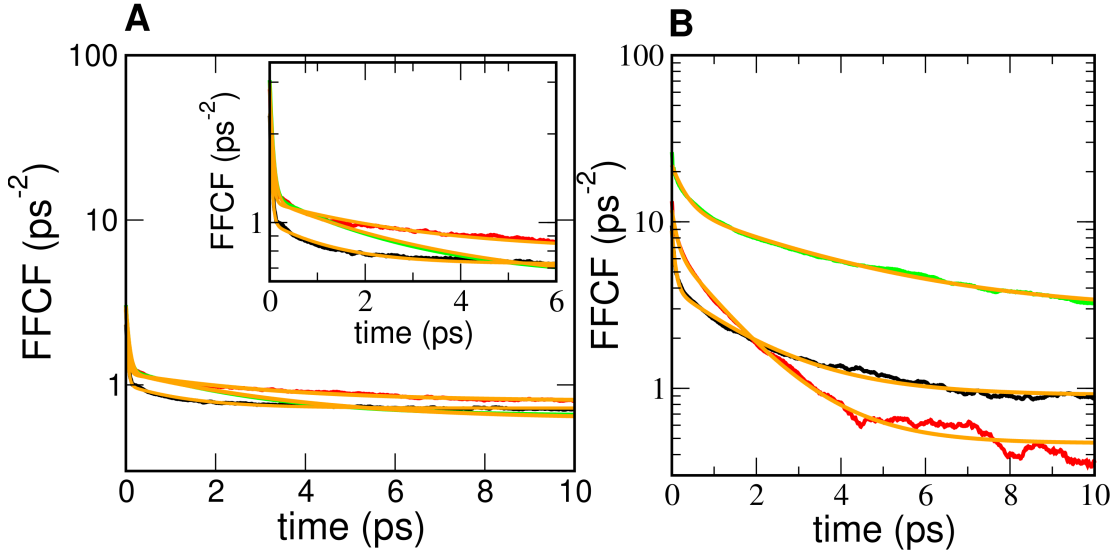


Figure 6: FFCF for each -CO moiety of trialanine using the MTP model (panel A) and from SCC-DFTB simulations (panel B) for central -CO (black), outer -CO (red), and the CO(OH) group (green). The orange lines are the fit to Eqn. 3 for each case.

The short time scale τ_1 ranges from 0.04 to 0.07 ps whereas the longer one ranges from 1.3 ps to 3.2 ps. Using PC simulations the decay time τ_1 is similar to that from the MTP simulation whereas the long time scales increase by about a factor of two. The amplitudes (a_1 and a_2)

of the two time scales are comparable for the two methods. For the simulation with MTPs, the static components for the central and outer amide are similar in magnitude, on average $\Delta_0^2 \sim 0.75 \text{ ps}^{-2}$ (which yields $\Delta_0 \sim 0.866 \text{ ps}^{-1}$ equivalent to $\Delta_0 = 4.6 \text{ cm}^{-1}$), which is in good agreement with the experimentally reported value³⁵ of $\Delta_0 = 5 \text{ cm}^{-1}$. This static component appears for (Ala)₃ but not for NMA and is quantitatively captured by using the MTP force field together with the FNM analysis and consistent with experiment which report that “In contrast to NMA, the amide I band of trialanine is still notably inhomogeneous on the 4 ps time scale.”³⁵ For the simulations with the PC model, the fits to Eq. 3 yield $\Delta_0^2 = 0.20 \text{ ps}^{-2}$ and $\Delta_0^2 = 0.42 \text{ ps}^{-2}$ which is smaller by about a factor of two compared with experiment. Also, the two static components for the central and outer -CO label differ by a factor of two.

With SCC-DFTB, the short time decay τ_1 is considerably slower (0.1 ps to 0.3 ps) and the longer time scales range from 1.4 ps to 3.5 ps. The short time decay is considerably longer than that reported from experiment whereas the long time decay for the central and outer -CO are compatible with $\tau_c = 1.6 \text{ ps}$ used for interpreting experiments on (Ala)₃ which was, however, fixed at the value found for NMA.³⁵ The values of Δ_0^2 for the central and outer -CO differ by a factor of two, similar to the results from the simulations with PCs but on average, they are consistent with the experimental value.³⁵

The magnitude of $C(t = 0)$ (i.e. the FFCF at $t = 0$) has been reported to be $\Delta_1^2 = 121 \text{ cm}^{-2}$ equivalent to 4.30 ps^{-2} .⁶¹ This compares with values of 1.65 ps^{-2} , 2.05 ps^{-2} , and 2.39 ps^{-2} from simulations with MTP and 8.5 ps^{-2} , 12.78 ps^{-2} , and 23.33 ps^{-2} , from the SCC-DFTB simulations for the central, outer and CO(OH) groups. Hence, the MTP simulations underestimate the experimentally reported amplitude whereas SCC-DFTB simulations overestimate it by about a factor of two. This was also found for simulations and experiments on fluoro-acetonitrile.⁶⁴ The value $C(t = 0)$ is a measure of the interaction strength between the reporter(s) and the environment. Thus, the present findings suggest that this interaction

is underestimated by the MTP model and overestimated by SCC-DFTB. Such information can be used to further improve the energy function.

Considering the results on the FFCFs for NMAD and (Ala)₃ together it is noted that only the simulations with MTP are consistent with experiment in that a) their decay times are close to one another and b) the fact that the FFCF for NMAD has no static component but that for (Ala)₃ has $\Delta_0^2 > 0$. It is also of interest to note that the fast decay time $\tau_1 \lesssim 100$ fs of the FFCF observed in the present simulations is consistent with an experimentally observed time constant of $\tau = 110 \pm 20$ fs.³⁶

The associated lineshapes for the three different modes involving the -CO stretch for trialanine are calculated via 1D Fourier transformation of the lineshape function as was done for NMAD, see Figures 5C and D. The FWHM for the 1D-IR spectra are 13 cm^{-1} for the central -CO, 17 cm^{-1} for the outer one and 18 cm^{-1} for the terminal -CO(OH) using the MTP model and 25 cm^{-1} , 32 cm^{-1} , and 50 cm^{-1} when using the SCC-DFTB model. Experimentally,⁶¹ it was found that the FWHM for NMAD and (Ala)₃ differ little and are $\sim 20 \text{ cm}^{-1}$. Both findings are quite well captured by the MTP simulations whereas with SCC-DFTB the widths are larger and differ somewhat more between NMAD and (Ala)₃.

Structural Dynamics: To characterize the structural dynamics afforded by the different energy functions used in the present work, the distribution of Φ/Ψ angles (Ramachandran plot) were determined from trajectories with the PC, MTP, and SCC-DFTB models, see Figure 7. This is used to determine whether, depending on the energy function used, the conformational space sampled differs. Also, assessing differences in the sampling between simulations in the gas phase and in solution are of interest. Both, the conventional $[\Phi, \Psi]$ map involving the central and outer -CO labels, and the dihedral angles for the terminal -CO are reported.

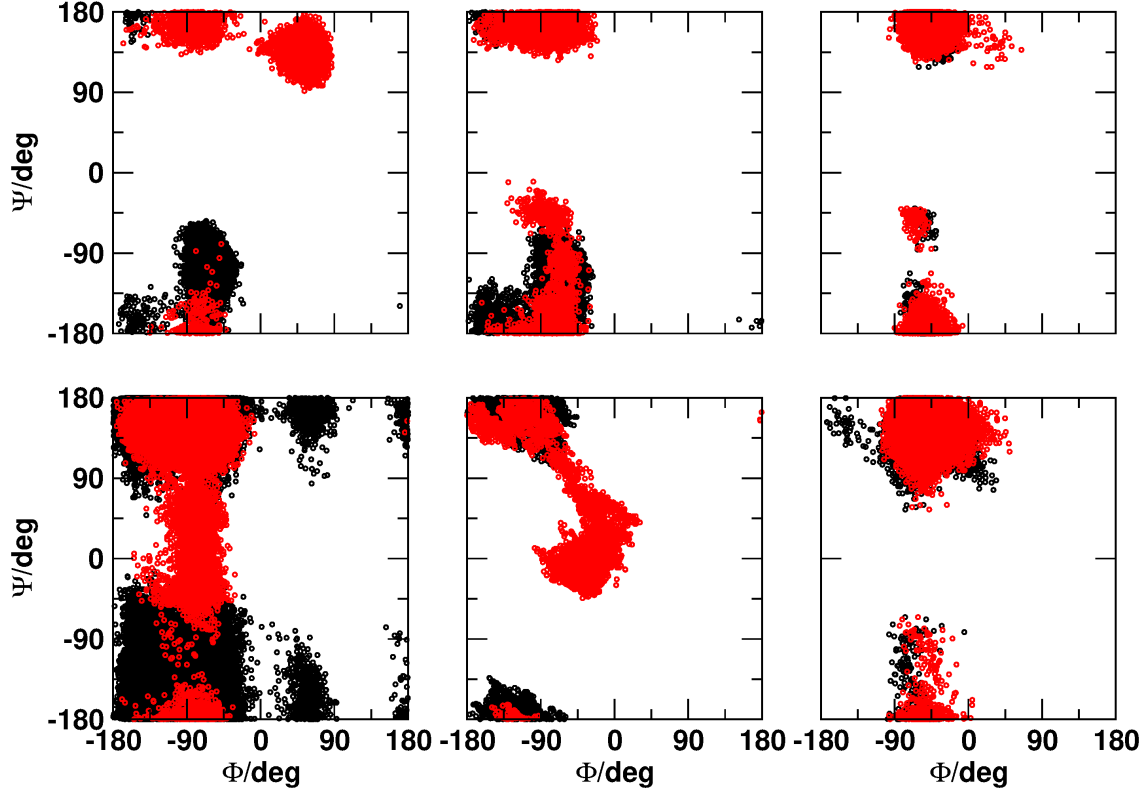


Figure 7: Ramachandran plots (Φ/Ψ angle) of trialanine using the PC (left panel), SCC-DFTB (middle panel) and MTP (right panel) models. Top and bottom panels are from simulations in the gas-phase and in water, respectively. Black are the Ramachandran angles, and red are the Φ/Ψ angles of trialanine for the carboxylic terminus. The centers for the $[\Phi, \Psi]$ angles for the β , P_{II} , α_R and α_L conformations are $[-140^\circ, 130^\circ]$, $[-75^\circ, 150^\circ]$, $[-70^\circ, -50^\circ]$, and $[50^\circ, 50^\circ]$, respectively.

Figure 7 shows the Ramachandran plot for trialanine from simulations using the PC (left panel), SCC-DFTB (middle panel) and MTP (right panel) models. The centers for the $[\Phi, \Psi]$ angles for the β , P_{II} , α_R and α_L conformations are $[-140^\circ, 130^\circ]$, $[-75^\circ, 150^\circ]$, $[-70^\circ, -50^\circ]$, and $[50^\circ, 50^\circ]$, respectively. From simulations in the gas phase (top) the distributions for the regular Ramachandran angles from PC and SCC-DFTB simulations are similar. They both sample β , P_{II} , and α_R structures. For simulations with MTP the densities are somewhat more shifted towards the P_{II} structures and the α_R state is sampled as well. For the COOH group (red), the region for $\Phi > 0$ is occupied for simulations with PCs but not with SCC-DFTB. For simulations with the MTP model the same regions as for the regular Ra-

ramachandran angles are sampled.

The distribution of conformational state population in Figure 7 find increased flexibility of (Ala)₃ from simulations with the PC model compared with those using MTP and SCC-DFTB both in the gas phase and in water. For the simulations in water (bottom row in Figure 7), the changes compared with the gas phase are most pronounced with PCs. In addition to the β , P_{II}, and α_R structures, the poly-Gly regions are also accessed extensively. Contrary to that, the differences between the gas and the condensed phase from simulations with SCC-DFTB and MTP are smaller but nevertheless exhibit increased flexibility as was found for the simulations with PCs. Using SCC-DFTB sampling of the β and P_{II} structures is extensive whereas α_R is not sampled at all for the regular Ramachandran angle (but for the -COOH terminus, see red distribution). Finally, for MTP, the distributions in the region of the β and P_{II} states broaden and there is also some limited sampling of the α_R helix. Both, SCC-DFTB and MTP only sample “allowed” regions in solution whereas PC also accesses “unusual” (poly-Gly) and “forbidden” regions.

Ramachandran maps have also been reported from simulations using a range of parametrized, PC-based force fields, including C27, C36, and C36m together with the TIP3P and SPC/E water models.⁴⁴ The distributions found in the present work, see Figure 7 lower left panel, are consistent with these (Φ, Ψ) maps. Using a Bayesian refinement on the measured and computed 1d-IR spectra, a consensus 2-dimensional potential of mean force (PMF) as a function of (Φ, Ψ) was determined. Notably, the refined PMF(Φ, Ψ) vis-a-vis experiment reported in Ref.⁴⁴ closely resembles the distribution found from the MTP simulations, see black symbols in Figure 7 lower right panel.

Table 3 summarizes state populations for β , P_{II}, α_R and α_L conformations of trialanine from simulations with PC, MTP, and SCC-DFTB models. A comparison with several previous

studies is also provided.^{34,37,39,40,42–44} For assigning a particular conformation to one of the 4 states, first centers (Φ , Ψ) of each of the states were defined as $[-140^\circ, 130^\circ]$, $[-75^\circ, 150^\circ]$, $[-70^\circ, -50^\circ]$, and $[50^\circ, 50^\circ]$ for β , P_{II} , α_R and α_L conformations, respectively. If a particular conformation is within $\pm 40^\circ$ around any of the centers, the conformation is assigned to that center. If a conformation is outside these bounds, it is not assigned which is the case for 30 % to 40 % of the structures. Then the percentage for the population of a particular substate was determined as the fraction of all assigned conformations. The present simulations using MTP find dominant population of the P_{II} state (98 %) with a small fraction of β and α_R . Using a PC model, P_{II} is still most populated, followed by β and α_R . Simulations with SCC-DFTB yield a higher population of β , a smaller fraction for P_{II} and no helical conformations.

Most previous studies find that the P_{II} state is most populated, typically followed by β structures. The relative populations range from 66 % to 92 % for P_{II} and 0 to 23 % for β . Fewer studies report population of α_R . One of the most sophisticated investigations (Bayesian ensemble refinement against FTIR and 2DIR experimental data)⁴⁴ report a $(85 \pm 6)\%$ population for P_{II} , $(14 \pm 5)\%$ for β and an insignificant population $(1 \pm 2)\%$ for α_R . Within error bars, the results from the MTP simulations are consistent with these findings. It is interesting to note that the “original” state populations in the work by Tokmakoff et al. were all derived from MD simulations using PC-based force fields and the populations are largely independent on the particular choice of the all-atom FF, see Table S5 in Ref.⁴⁴ Specifically, the populations from the C36 parametrization with the TIP3P water model (as used here, see Table S4 in Ref.⁴⁴) compare favourably with the present findings for β structures (18% vs. 20 %), P_{II} (68 % vs. 79 %), and α_R . (6 % vs. 3%). Differences may arise due to slightly different definitions of the basins to integrate the populations and whether or not all of the conformations are used for analysis. After Bayesian refinement the populations are comparable to those from MTP simulations. In other words, machine learning of the populations based on the comparison of measured and computed IR spectra has the same

effect as replacement of PCs by MTPs in the present simulations, lending additional support to the physical relevance afforded by the anisotropic effects in the electrostatic interactions.

Table 3: State population for β , P_{II} , α_R and α_L conformations of trialanine from simulations with PC, MTP, and SCC-DFTB compared with previously reported values. ^aMD simulation, ^bBayesian ensemble refinement against FTIR and 2D IR, ^cFitting 2D IR spectra, ^dFitting VCD, Raman, FTIR and J-coupling, ^eFitting NMR, ^fFitting NMR with Gromos 43A1, ^gFitting NMR with integrated Bayesian approach, ^hBayesian energy landscape tilting. The standard deviation from the average is given in parentheses.

Conformational State Population				
	β	P_{II}	α_R	α_L
MTP (this work)	1%	98%	1%	0
PC (this work)	18%	79%	3%	<1%
SCC-DFTB (this work)	62%	38%	0	0
Tokmakoff et al. (original) ^{44,a}	(22 ± 7)%	(63 ± 11)%	(12 ± 8)%	(3 ± 2)%
Tokmakoff et al. (Refined) ^b	(14 ± 5)%	(85 ± 6)%	(1 ± 2)%	< 0.1%
Woutersen et al. ^{34,c}	0%	80%	20%	0%
Mu et al. ³⁹	42%	41%	16%	0.8%
Schweitzer-Stenner ^{37,d}	16%	84%	0%	0%
Graf et al. ^{40,e}	8%	92%	0%	0%
Oh et al. ^{42,f}	12%	88%	0%	0%
Xiao et al. ^{43,g}	2.0 ± 1.8)%	(85.8 ± 4.9)%	(5.5 ± 4.1)%	(3.5 ± 2.7)%
Beauchamp et al. ^{75,h}	(23 ± 6)%	(67 ± 9)%	(10 ± 8)%	—

FFCF from Independent Normal Modes

The amide-I vibrational dynamics encoded in the FFCF contains information about the solvent dynamics as well as the peptide conformational dynamics. To better understand the influence of inter-mode couplings on the conformational dynamics, the instantaneous normal modes for the central and the outer -CO label were also determined from normal mode analyses treating the two amide modes independently. This is then compared with the FFCFs obtained from the FNM analysis which contains the couplings between the labels.

The FFCFs for the central and the outer -CO from INM (dashed lines) and from FNM (solid

lines) are reported in Figure 8 and the fitting parameters to Eq. 3 using two time scales are given in Table 2. Without coupling (dashed lines) the FFCFs decay close to zero on the 10 ps time scale and the magnitude of Δ_0^2 decreases by almost one order of magnitude compared with the results from FNM. Also, the decay times are shorter if the coupling between the two labels is neglected. As the results from FNM analysis agree with experiment and those omitting the coupling do not, it is concluded that the FNM analysis together with a MTP representation of the electrostatics provides a means to correctly describe the dynamics of hydrated (Ala)₃.

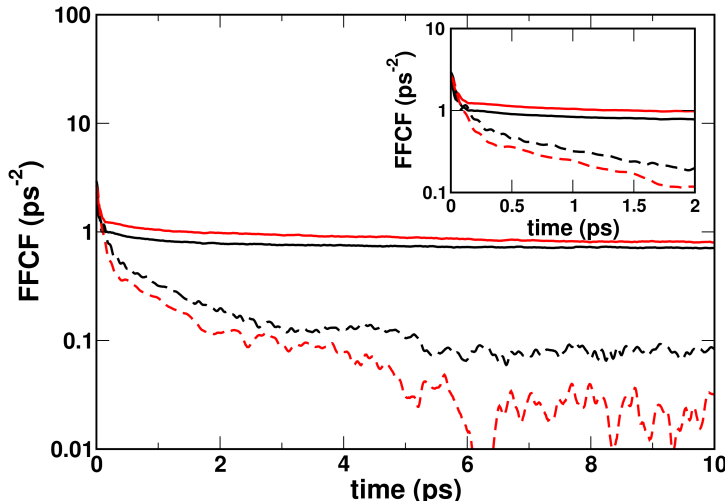


Figure 8: Comparison of FFCFs from full NM analysis (solid lines) and independent NM analysis (dashed lines) for the outer (red) and central (black) amide modes of trialanine.

Including couplings between the labels (“sites”) is also important when working with map-based approaches for 1d- and 2d-IR spectroscopy.^{33,76,77} Using frequency maps, the site energies, the nearest neighbor coupling and the transition dipole couplings are usually included in the excitonic Hamiltonian.³³ Such couplings need to be (re-)introduced in an excitonic Hamiltonian but they are already partly present in the FNM approach used here, as the above analysis demonstrates. The molecular dynamics simulations which generate the conformational ensemble to be analyzed include couplings through the nuclear dynamics and the

FNM analysis preserves these couplings whereas the INM analysis almost entirely removes them.

Comparing the maxima of the peak positions from the frequency distributions based on “full NM” and “independent NM” reveals that the two analyses differ in capturing this coupling. From INM the frequency distributions peak at 1661.5 cm^{-1} and 1662 cm^{-1} , i.e. a splitting of close to zero, whereas from FNM the maxima are at 1670 cm^{-1} and 1683 cm^{-1} , i.e. a splitting of 13 cm^{-1} . Within a simple two-state Hamiltonian this amounts to a coupling of $\sim 6.5\text{ cm}^{-1}$, consistent with experiments.³⁶

The finite amplitude of Δ_0^2 is also indicative of the fact that within the explored time scale the system has not exhaustively sampled all available states. In other words, population relaxation is not complete on the 10 ps time scale. This is consistent with an analysis of MD trajectories that determined the FFCF from only sampling the P_{II} conformation (which decays to zero on the $\sim 4\text{ ps}$ time scale) compared with the full MD trajectory sampling different substates for which a static contribution remains even after 10 ps.⁶¹ This interpretation is also consistent with the fact that NMAD only has one conformational substate and therefore the FFCF decays to zero on the 10 ps time scale.

Summary and Conclusion

In summary, the present work provides a comprehensive assessment and comparison of the dynamics and infrared spectroscopy of NMAD and $(\text{Ala})_3$ in D_2O . Consistent with experiments on $(\text{Ala})_3$ it is found that with “full normal modes” from simulations using MTPs to compute the frequency trajectory, the 1d-infrared spectrum for the outer and central -CO labels are split by 13 cm^{-1} , compared with 25 cm^{-1} from experiment. With independent normal modes this splitting is close to zero. Including the site-site couplings in the NM

analysis therefore yields a more quantitative description of the spectroscopy and dynamics. This splitting is larger (47 cm^{-1}) in simulations with SCC-DFTB for the solute. The FFCF from FNM has an initial amplitude $C(t = 0)$ of $[1.65, 2.05]\text{ ps}^{-2}$ for the central and outer -CO label, compared with 4.30 ps^{-2} from experiment and $[8.5, 12.78]\text{ ps}^{-2}$ from simulations with SCC-DFTB. This points towards somewhat weaker interactions of the -CO labels with the environment in the MTP simulations and a considerably stronger interaction in SCC-DFTB. The long-time static component from MTP simulations with FNM of $\Delta_0 = 4.6\text{ cm}^{-1}$ compares well with that observed experimentally ($\Delta_0 = 5.0\text{ cm}^{-1}$) whereas that from simulations with PCs is smaller by a factor of two. The MTP simulations find comparable values for Δ_0 for the central and outer -CO whereas with SCC-DFTB they differ by about a factor of two with one of the values $\sim 20\%$ larger than that observed experimentally and the other one lower by a similar amount, see Table 2.

Overall, simulations for $(\text{Ala})_3$ with MTP and FNM analysis find good to quantitative agreement with experiment for the splitting, amplitude of $C(t = 0)$, and value for Δ_0 . This contrasts with simulations using PC and/or INM or SCC-DFTB simulations. The conformational space sampled by $(\text{Ala})_3$ in solution is dominated by a P_{II} structure (98 %), followed by β and α_R , each populated in 1 % of the cases. This agrees qualitatively with a Bayesian refined analysis⁴⁴ of recent infrared experiments which find occupations of $[P_{II}, \beta, \alpha_R]$ $[85 \pm 6, 14 \pm 5, 1 \pm 2]\%$ but differ somewhat from earlier results³⁴ which report $[80, 0, 20]\%$.

The present work demonstrates that the structural dynamics of a small, hydrated peptide can be correctly described from MD simulations based on an MTP force field in explicit solvent together with a full normal mode analysis. Such studies provide the necessary basis to link structural dynamics, spectroscopy and aggregation in larger proteins from experiment and simulations.

Acknowledgments

The authors gratefully acknowledge financial support from the Swiss National Science Foundation through grant 200021-117810 and to the NCCR-MUST. The authors thank Prof. Peter Hamm for valuable discussions.

References

- (1) Ganim, Z.; Chung, H. S.; Smith, A. W.; DeFlores, L. P.; Jones, K. C.; Tokmakoff, A. Amide I two dimensional infrared spectroscopy of proteins. *Acc. Chem. Res.* **2008**, *41*, 432–441.
- (2) Getahun, Z.; Huang, C. Y.; Wang, T.; Leon, B. D.; DeGrado, W. F.; Gai, F. Using Nitrile-Derivatized Amino Acids as Infrared Probes of Local Environment. *J. Am. Chem. Soc.* **2003**, *125*, 405–411.
- (3) Bagchi, S.; Boxer, S. G.; Fayer, M. D. Ribonuclease S Dynamics Measured Using a Nitrile Label with 2D IR Vibrational Echo Spectroscopy. *J. Phys. Chem. B* **2012**, *116*, 4034–4042.
- (4) Xu, L.; Cohen, A. E.; Boxer, S. G. Electrostatic Fields near the Active Site of Human Aldose Reductase: 2. New Inhibitors and Complications Caused by Hydrogen Bonds. *Biochem.* **2011**, *50*, 8311–8322.
- (5) Mondal, P.; Meuwly, M. Vibrational Stark Spectroscopy for Assessing Ligand-Binding Strength in a Protein. *Phys. Chem. Chem. Phys.* **2017**, *19*, 16131–16143.
- (6) Bloem, R.; Koziol, K.; Waldauer, S. A.; Buchli, B.; Walser, R.; Samatanga, B.; Jele-sarov, I.; Hamm, P. Ligand Binding Studied by 2D IR Spectroscopy Using the Azido-homoalanine Label. *J. Phys. Chem. B* **2012**, *116*, 13705–13712.

- (7) Layfield, J. P.; Hammes-Schiffer, S. Calculation of Vibrational Shifts of Nitrile Probe in the Active Site of Ketosteroid Isomerase upon Ligand Binding. *J. Am. Chem. Soc.* **2013**, *135*, 717–725.
- (8) Salehi, S. M.; Koner, D.; Meuwly, M. Dynamics and Infrared Spectroscopy of Monomeric and Dimeric Wild Type and Mutant Insulin. *J. Phys. Chem. B* **2020**, *124*, 11882–11894.
- (9) Waegle, M. M.; Culik, R. M.; Gai, F. Site-Specific Spectroscopic Reporters of the Local Electric Field, Hydration, Structure, and Dynamics of Biomolecules. *J. Phys. Chem. Lett.* **2011**, *2*, 2598–2609.
- (10) Koziol, K. L.; Johnson, P. J. M.; Stucki-Buchli, B.; Waldauer, S. A.; Hamm, P. Fast infrared spectroscopy of protein dynamics: advancing sensitivity and selectivity. *Curr. Op. Struct. Biol.* **2015**, *34*, 1–6.
- (11) Horness, R. E.; Basom, E. J.; Thielges, M. C. Site-selective characterization of Src homology 3 domain molecular recognition with cyanophenylalanine infrared probes. *Anal. Chem.* **2015**, *7*, 7234–7241.
- (12) Getahun, Z.; Huang, C.; Wang, T.; De Leon, B.; DeGrado, W.; Gai, F. Using nitrile-derivatized amino acids as infrared probes of local environment. *J. Am. Chem. Soc.* **2003**, *125*, 405–411.
- (13) Kozinski, M.; Garrett-Roe, S.; Hamm, P. 2D-IR spectroscopy of the sulfhydryl band of cysteines in the hydrophobic core of proteins. *J. Phys. Chem. B* **2008**, *112*, 7645–7650.
- (14) Zimmermann, J.; Thielges, M. C.; Yu, W.; Dawson, P. E.; Romesberg, F. E. Carbon-Deuterium Bonds as Site-Specific and Nonperturbative Probes for Time-Resolved Studies of Protein Dynamics and Folding. *J. Phys. Chem. Lett.* **2011**, *2*, 412–416.

- (15) Woys, A. M.; Mukherjee, S. S.; Skoff, D. R.; Moran, S. D.; Zanni, M. T. A Strongly Absorbing Class of Non-Natural Labels for Probing Protein Electrostatics and Solvation with FTIR and 2D IR Spectroscopies. *J. Phys. Chem. B* **2013**, *117*, 5009–5018.
- (16) Bagchi, S.; Boxer, S. G.; Fayer, M. D. Ribonuclease S Dynamics Measured Using a Nitrile Label with 2D IR Vibrational Echo Spectroscopy. *J. Phys. Chem. B* **2012**, *116*, 4034–4042.
- (17) Zimmermann, J.; Thielges, M. C.; Seo, Y. J.; Dawson, P. E.; Romesberg, F. E. Cyano Groups as Probes of Protein Microenvironments and Dynamics. *Angew. Chem. Int. Ed.* **2011**, *50*, 8333–8337.
- (18) van Wilderen, L. J. G. W.; Kern-Michler, D.; Mueller-Werkmeister, H. M.; Bredenbeck, J. Vibrational dynamics and solvatochromism of the label SCN in various solvents and hemoglobin by time dependent IR and 2D-IR spectroscopy. *Phys. Chem. Chem. Phys.* **2014**, *16*, 19643–19653.
- (19) Lee, G.; Kossowska, D.; Lim, J.; Kim, S.; Han, H.; Kwak, K.; Cho, M. Cyanamide as an Infrared Reporter: Comparison of Vibrational Properties between Nitriles Bonded to N and C Atoms. *J. Phys. Chem. B* **2018**, *122*, 4035–4044.
- (20) Hamm, P.; Zanni, M. *Concept and Methods of 2D Infrared Spectroscopy*; Cambridge University Press, 2011.
- (21) Hamm, P.; Lim, M.; Hochstrasser, R. Structure of the Amide I Band of Peptides Measured by Femtosecond Nonlinear-Infrared Spectroscopy. *J. Phys. Chem. B* **1998**, *5647*, 6123–6138.
- (22) Zanni, M. T.; Asplund, M. C.; Hochstrasser, R. Two Dimensional Heterodyned and Stimulated Infrared Photon Echoes of N-Methylacetamide-D. *J. Chem. Phys.* **2001**, *114*, 4579–4590.

- (23) Woutersen, S.; Mu, Y.; Stock, G.; Hamm, P. Hydrogen-bond lifetime measured by time-resolved 2D-IR spectroscopy: N-methylacetamide in methanol. *Chem. Phys.* **2001**, *266*, 137–147.
- (24) Wang, L.; Middleton, C. T.; Zanni, M. T.; Skinner, J. L. Development and Validation of Transferable Amide I Vibrational Frequency Maps for Peptides. *J. Phys. Chem. B* **2011**, *115*, 3713–3724.
- (25) Cazade, P.-A.; Bereau, T.; Meuwly, M. Computational Two-Dimensional Infrared Spectroscopy without Maps: N-Methylacetamide in Water. *J. Phys. Chem. B* **2014**, *118*, 8135–8147.
- (26) Yadav, V. K.; Chandra, A. First-principles simulation study of vibrational spectral diffusion and hydrogen bond fluctuations in aqueous solution of N-methylacetamide. *J. Phys. Chem. B* **2015**, *119*, 9858–9867.
- (27) Gaigeot, M. P.; Vuilleumier, R.; Sprik, M.; Borgis, D. Infrared Spectroscopy of N-Methylacetamide Revisited by ab initio Molecular Dynamics Simulations. *J. Chem. Theo. Comp.* **2005**, *1*, 772–789.
- (28) Cazade, P.-A.; Meuwly, M. Oxygen Migration Pathways in NO-bound Truncated Hemoglobin. *Chem. Phys. Chem.* **2012**, 4276–4286.
- (29) Koziol, K. L.; Johnson, P. J. M.; Stucki-Buchli, B.; Waldauer, S. A.; Hamm, P. Fast Infrared Spectroscopy of Protein Dynamics: Advancing Sensitivity and Selectivity. *Curr. Op. Struct. Biol.* **2015**, *34*, 1–6.
- (30) Cho, M.; Fleming, G. R.; Saito, S.; Ohmine, I.; Stratt, R. M. Instantaneous normal mode analysis of liquid water. *J. Chem. Phys.* **1994**, *100*, 6672–6683.
- (31) Salehi, S. M.; Koner, D.; Meuwly, M. Vibrational Spectroscopy of N_3^- in the Gas and Condensed Phase. *J. Phys. Chem. B* **2019**, *123*, 3282–3290.

- (32) Koner, D.; Salehi, M.; Mondal, P.; Meuwly, M. Non-conventional Force Fields for Applications in Spectroscopy and Chemical Reaction Dynamics. *J. Chem. Phys.* **2020**, *153*, 10901–10912.
- (33) Wang, L.; Middleton, C. T.; Zanni, M. T.; Skinner, J. L. Development and Validation of Transferable Amide I Vibrational Frequency Maps for Peptides. *J. Phys. Chem. B* **2011**, *115*, 3713–3724.
- (34) Woutersen, S.; Hamm, P. Structure Determination of Trialanine in Water Using Polarization Sensitive Two-Dimensional Vibrational Spectroscopy. *J. Phys. Chem. B* **2000**, *104*, 11316–11320.
- (35) Woutersen, S.; Pfister, R.; Hamm, P.; Mu, Y.; Kosov, D. S.; Stock, G. Peptide Conformational Heterogeneity Revealed from Nonlinear Vibrational Spectroscopy and Molecular-Dynamics Simulations. *J. Chem. Phys.* **2002**, *117*, 6833–6840.
- (36) Woutersen, S.; Mu, Y.; Stock, G.; Hamm, P. Subpicosecond conformational dynamics of small peptides probed by two-dimensional vibrational spectroscopy. *Proc. Natl. Acad. Sci.* **2001**, *98*, 11254–11258.
- (37) Schweitzer-Stenner, Q. H. R.; Eker, F.; Griebenov, K. Dihedral Angles of Trialanine in D₂O Determined by Combining FTIR and Polarized Visible Raman Spectroscopy. *J. Am. Chem. Soc.* **2001**, *123*, 9628–9633.
- (38) Woutersen, S.; Hamm, P. Isotope-edited two-dimensional vibrational spectroscopy of trialanine in aqueous solution. *J. Chem. Phys.* **2001**, *114*, 2727–2737.
- (39) Mu, Y.; Stock, G. Conformational Dynamics of Trialanine in Water : A Molecular Dynamical Study. *J. Phys. Chem. B* **2002**, *106*, 5294–5301.
- (40) Graf, J.; Nguyen, P. H.; Schwalbe, H. Structure and dynamics of the homologous series

- of alanine peptides: a joint molecular dynamics/NMR study. *J. Am. Chem. Soc.* **2007**, *129*, 1179–1189.
- (41) Gorbunov, R. D.; Nguyen, P. H.; Kobus, M.; Stock, G. Quantum-classical description of the amide I vibrational spectrum of trialanine. *J. Chem. Phys.* **2007**, *126*, 02B601.
- (42) Oh, K. I.; Lee, K. K.; Cho, M. Circular dichroism eigen spectra of polyproline II and β -strand conformers of trialanine in water: singular value decomposition analysis. *Chirality* **2010**, *22*, E186–E201.
- (43) Xiao, X.; Kallenbach, N.; Zhang, Y. Peptide conformation analysis using an integrated Bayesian approach. *J. Chem. Theo. Comput.* **2014**, *10*, 4152–4159.
- (44) Feng, C. J.; Dhayalan, B.; Tokmakoff, A. Refinement of Peptide Conformational Ensembles by 2D IR Spectroscopy: Application to Ala–Ala–Ala. *Biophys. J.* **2018**, *114*, 2820–2832.
- (45) Jorgensen, W. L.; Chandrasekhar, J.; Madura, J. D.; Impey, R. W.; Klein, M. L. Comparison of Simple Potential Functions for Simulating Liquid Water. *J. Chem. Phys.* **1983**, *79*, 926–935.
- (46) Brooks, B. R.; Brooks, C. L., III; Mackerell, A. D., Jr.; Nilsson, L.; Petrella, R. J.; Roux, B.; Won, Y.; Archontis, G.; Bartels, C.; Boresch, S. et al. CHARMM: The Biomolecular Simulation Program. *J. Comp. Chem.* **2009**, *30*, 1545–1614.
- (47) Bereau, T.; Kramer, C.; Meuwly, M. Leveraging Symmetries of Static Atomic Multipole Electrostatics in Molecular Dynamics Simulations. *J. Chem. Theo. Comp.* **2013**, *9*, 5450–5459.
- (48) Kramer, C.; Gedeck, P.; Meuwly, M. Atomic Multipoles: Electrostatic Potential Fit, Local Reference Axis Systems and Conformational Dependence. *J. Comp. Chem.* **2012**, *33*, 1673–1688.

- (49) Vanommeslaeghe, K.; Hatcher, E.; Acharya, C.; Kundu, S.; Zhong, S.; Shim, J.; Darian, E.; Guvench, O.; Lopes, P.; Vorobyov, I. et al. CHARMM General Force Field: A Force Field for Drug-Like Molecules Compatible with the CHARMM All-Atom Additive Biological Force Fields. *J. Comp. Chem.* **2010**, *31*, 671–690.
- (50) Darden, T.; York, D.; Pedersen, L. Particle mesh Ewald: An Nlog(N) method for Ewald sums in large systems. *J. Chem. Phys.* **1993**, *98*, 10089–10092.
- (51) van Gunsteren, W.; Berendsen, H. Algorithms for Macromolecular Dynamics and Constraint Dynamics. *Mol. Phys.* **1977**, *34*, 1311–1327.
- (52) Elstner, M.; Porezag, D.; Jungnickel, G.; Elsner, J.; Haugk, M.; Frauenheim, T.; Suhai, S.; Seifert, G. Self-consistent-charge density-functional tight-binding method for simulations of complex materials properties. *Phys. Rev. B* **1998**, *58*, 7260–7268.
- (53) Cui, Q.; Elstner, M.; Kaxiras, E.; Frauenheim, T.; Karplus, M. A QM/MM Implementation of the Self-Consistent Charge Density Functional Tight Binding (SCC-DFTB) Method. *J. Phys. Chem. B* **2001**, *105*, 569–585.
- (54) Vanommeslaeghe, K.; Hatcher, E.; Acharya, C.; Kundu, S.; Zhong, S.; Shim, J.; Darian, E.; Guvench, O.; Lopes, P.; Vorobyov, I. et al. CHARMM General Force Field (CGenFF): A force field for drug-like molecules compatible with the CHARMM all-atom additive biological force fields. *J. Comp. Chem.* **2010**, *31*, 671–690.
- (55) Salehi, S. M.; Meuwly, M. Site-selective dynamics of azidolysosome. *J. Chem. Phys.* **2021**, *154*, 165101.
- (56) Adams, J. E.; Stratt, R. M. Instantaneous Normal Mode Analysis as a Probe of Cluster Dynamics. *J. Chem. Phys.* **1990**, *93*, 1332–1346.
- (57) Buchner, M.; Ladanyi, B. M.; Stratt, R. M. The Short-Time Dynamics of Molecular Liquids-Instantaneous-Normal-Mode Theory. *J. Chem. Phys.* **1992**, *97*, 8522–8535.

- (58) Bastida, A.; Soler, M. A.; Zuniga, J.; Requena, A.; Kalstein, A.; Fernandez-Alberti, S. Instantaneous normal modes, resonances, and decay channels in the vibrational relaxation of the amide I mode of N-methylacetamide-D in liquid deuterated water. *J. Chem. Phys.* **2010**, *132*, 224501.
- (59) Sun, X.; Stratt, R. M. How a solute-pump/solvent-probe spectroscopy can reveal structural dynamics: Polarizability response spectra as a two-dimensional solvation spectroscopy. *J. Chem. Phys.* **2013**, *139*, 044506.
- (60) Schmidt, J.; Roberts, S.; Loparo, J.; Tokmakoff, A.; Fayer, M.; Skinner, J. Are water simulation models consistent with steady-state and ultrafast vibrational spectroscopy experiments? *Chem. Phys.* **2007**, *341*, 143–157.
- (61) Woutersen, S.; Pfister, R.; Hamm, P.; Mu, Y.; Kosov, D.; Stock, G. Peptide conformational heterogeneity revealed from nonlinear vibrational spectroscopy and molecular-dynamics simulations. *J. Chem. Phys.* **2002**, *117*, 6833–6840.
- (62) Decamp, M. F.; Deflores, L.; Mccracken, J. M.; Tokmakoff, A.; Kwac, K.; Cho, M. Amide I Vibrational Dynamics of N-Methylacetamide in Polar Solvents: The Role of Electrostatic Interaction. *J. Phys. Chem. B* **2005**, *109*, 11016–11026.
- (63) Laage, D.; Stirnemann, G.; Sterpone, F.; Rey, R.; Hynes, J. T. Reorientation and allied dynamics in water and aqueous solutions. **2011**, *62*, 395–416.
- (64) Cazade, P. A.; Tran, H.; Bereau, T.; Das, A. K.; Si, K.; Hamm, P.; Meuwly, M. Solvation of fluoro-acetonitrile in water by 2D-IR spectroscopy : A combined experimental-computational study. *J. Chem. Phys.* **2015**, *142*, 212415–212424.
- (65) Kubelka, J.; Keiderling, T. *Ab Initio* Calculation of Amide Carbonyl Stretch Vibrational Frequencies in Solution with Modified Basis Sets. 1. N-methyl Acetamide. *J. Phys. Chem. A* **2001**, *105*, 10922–10928.

- (66) Jones, R. L. The infrared spectra of some simple N-substituted amides in the vapor state. *J. Mol. Spectrosc.* **1963**, *11*, 411–421.
- (67) Devereux, M.; Raghunathan, S.; Fedorov, D. G.; Meuwly, M. A novel, computationally efficient multipolar model employing distributed charges for molecular dynamics simulations. *J. Chem. Theo. Comp.* **2014**, *10*, 4229–4241.
- (68) Unke, O. T.; Devereux, M.; Meuwly, M. Minimal distributed charges: Multipolar quality at the cost of point charge electrostatics. *J. Chem. Phys.* **2017**, *147*, 161712.
- (69) Nutt, D. R.; Meuwly, M. Theoretical investigation of infrared spectra and pocket dynamics of photodissociated carbonmonoxy myoglobin. *Biophys. J.* **2003**, *85*, 3612–3623.
- (70) Nutt, D. R.; Meuwly, M. Migration in native and mutant myoglobin: Atomistic simulations for the understanding of protein function. *Proc. Natl. Acad. Sci.* **2004**, *101*, 5998–6002.
- (71) Plattner, N.; Meuwly, M. Higher order multipole moments for molecular dynamics simulations. *J. Mol. Model.* **2009**, *15*, 687–94.
- (72) Plattner, N.; Meuwly, M. The role of higher CO-multipole moments in understanding the dynamics of photodissociated carbonmonoxide in myoglobin. *Biophys. J.* **2008**, *94*, 2505–2515.
- (73) Krüger, T.; Elstner, M.; Schiffels, P.; Frauenheim, T. Validation of the density-functional based tight-binding approximation method for the calculation of reaction energies and other data. *J. Chem. Phys.* **2005**, *122*, 114110.
- (74) Gaus, M.; Goez, A.; Elstner, M. Parametrization and benchmark of DFTB3 for organic molecules. *J. Chem. Theo. Comp.* **2013**, *9*, 338–354.
- (75) Beauchamp, K. A.; Pande, V. S.; Das, R. Bayesian energy landscape tilting: towards concordant models of molecular ensembles. *BioPhys. J.* **2014**, *106*, 1381–1390.

- (76) Jansen, T. I. C.; Dijkstra, A. G.; Watson, T. M.; Hirst, J. D.; Knoester, J. Modeling the amide I bands of small peptides. *J. Chem. Phys.* **2006**, *125*, 044312.
- (77) Reppert, M.; Tokmakoff, A. Electrostatic frequency shifts in amide I vibrational spectra: Direct parameterization against experiment. *J. Chem. Phys.* **2013**, *138*, 134116.